

Particle Physics Research Centre
School of Physics and Astronomy
Queen Mary University of London

Measurements of $H \rightarrow b\bar{b}$ decays and VH production

Thomas Charman

Supervisor: Dr. Jonathan Hays

Submitted in partial fulfillment of the requirements of the Degree of Doctor of Philosophy May 19, 2020.

I, Thomas Paul Charman, confirm that the research included within this thesis is my own work or that where it has been carried out in collaboration with, or supported by others, that this is duly acknowledged below and my contribution indicated. Previously published material is also acknowledged below.

I attest that I have exercised reasonable care to ensure that the work is original, and does not to the best of my knowledge break any UK law, infringe any third party's copyright or other Intellectual Property Right, or contain any confidential material.

I accept that the College has the right to use plagiarism detection software to check the electronic version of the thesis. I confirm that this thesis has not been previously submitted for the award of a degree by this or any other university.

The copyright of this thesis rests with the author and no quotation from it or information derived from it may be published without the prior written consent of the author.

Signature:

Date:

Details of collaboration and publications:

Contents

List of Figures	4
List of Tables	5
1 The ATLAS Detector at the Large Hadron Collider	6
1.1 The Large Hadron Collider	6
1.2 The ATLAS Detector	11
Inner Detector	14
Pixel Detectors	15
Semiconductor Tracker	15
Transition Radiation Tracker	17
Calorimeters	17
Electromagnetic Calorimeter	17
Hadronic Calorimeter	18
Muon Spectrometers	18
Trigger Systems	19

List of Figures

1.1	The CERN accelerator complex	7
1.2	A representation of a pair of idealised cylindrical magnets in a dipole configuration. Two positively charged particles are shown as circles, the red particle is traveling out of the page, the green particle is traveling into the page. The forces experienced by each particle due to the magnetic field are shown as blue arrows.	8
1.3	A representation of a radio-frequency cavity where the electric field lines are shown in black.	9
1.4	Representation of an idealised set of coil magnets in a quadrupole configuration with a proton beamspot shown as a red ellipse. The proton beam is drawn coming out of the page (<i>watch out!</i>), magnetic field lines are drawn in black and the forces acting on each bunch of protons are drawn as blue arrows.	10
1.5	The ATLAS Detector	11
1.6	ATLAS magnetic field	13
1.7	ATLAS inner detector	14
1.8	ATLAS long strip module	16
1.9	ATLAS strip close-up	16
1.10	ATLAS Calorimeter	18

1.11 ATLAS muon subsystem	19
-------------------------------------	----

List of Tables

Chapter 1

The ATLAS Detector at the Large Hadron Collider

1.1 The Large Hadron Collider

The Large Hadron Collider (LHC) [1] is a large circular machine located 100 m underground straddling the Swiss-French border at the European Organisation for Nuclear Research (CERN). The LHC accelerates and collides protons and other charged particles. It has a diameter of 27 km and resides in a tunnel which was originally excavated for the Large Electron-Positron Collider [2] experiment. During its construction the tunnel was the largest civil engineering project in Europe to date. Today there are many physics experiments that take place at CERN, some of which are marked in figure. 1.1. There are currently seven experiments that record data from the collisions at the LHC: ATLAS [3], CMS [4], LHCb [5], ALICE [6], MoEDAL [7], TOTEM [8] and LHCf [9].

The Lorentz force is fundamental to the LHC's accelerator technologies and detectors. Expressed as

$$\vec{F} = q(\vec{E} + \vec{v} \times \vec{B}), \quad (1.1)$$

it is clear that the force due to an electric field \vec{E} on a particle with charge q acts in the direction of the velocity of the field whereas the force due to a magnetic field \vec{B}

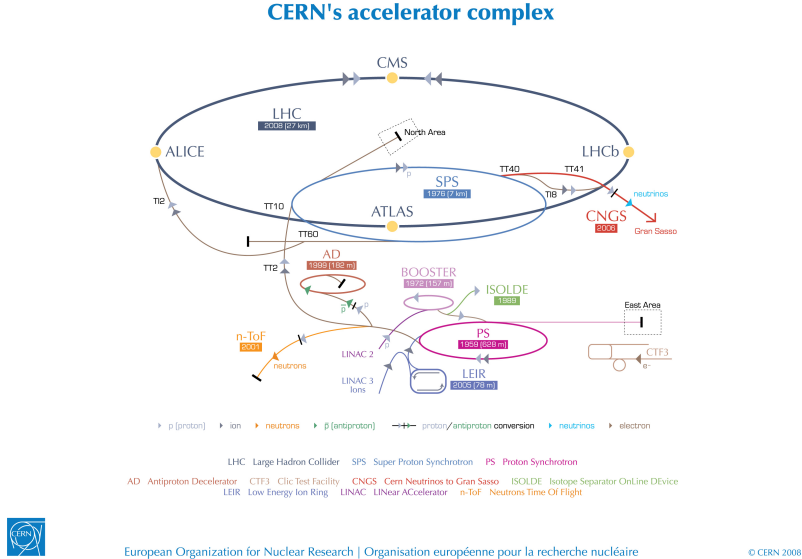


Figure 1.1: The CERN accelerator complex [10].

acts perpendicular to both the field and the velocity of the particle \vec{v} . It is therefore clear that an electric field may be used to accelerate and give energy to a charged particle whereas a magnetic field will alter the trajectory of a particle whilst keeping its energy constant.

The LHC is a Synchrotron, an accelerator that uses magnets in a dipole configuration, such as in figure 1.2, to bend the path of charged particles into conformity with its circular shape. It is apart from studying the figure that counter-rotating beams of same sign charged particles will require two sets of dipole magnets in order to rotate in opposite directions around the same ring. This is one disadvantage of a proton-proton collider with respect to a proton-anti-proton collider such as the Tevatron [?]. The bending magnets of a Synchrotron are designed to ramp up their magnetic field in synchronisation with the kinetic energy of the accelerated particles, allowing higher energies to be achieved before the beam is lost. The LHC can accelerate each beam to an energy of 6.5 TeV leading to collisions with a centre of mass energy of $\sqrt{s} = 13$ TeV, although the design energy of the LHC is $\sqrt{s} = 14$ TeV centre of mass energy of The LHC has 1232 dipole magnets [1] which are made of copper-clad niobium-titanium cables, a

superconducting material whose electrical resistance falls to zero at a threshold temperature. In order to maintain super-conductivity a cryogenic system using

liquid helium is employed to cool the magnets. The higher the velocity of a charged particle, and the tighter the desired bending radius, the larger the magnetic field required to perform the bending. The large size of the LHC and the choice of superconducting magnet technologies are both informed by the aim to accelerate protons to the highest energy, and therefore velocity, possible.

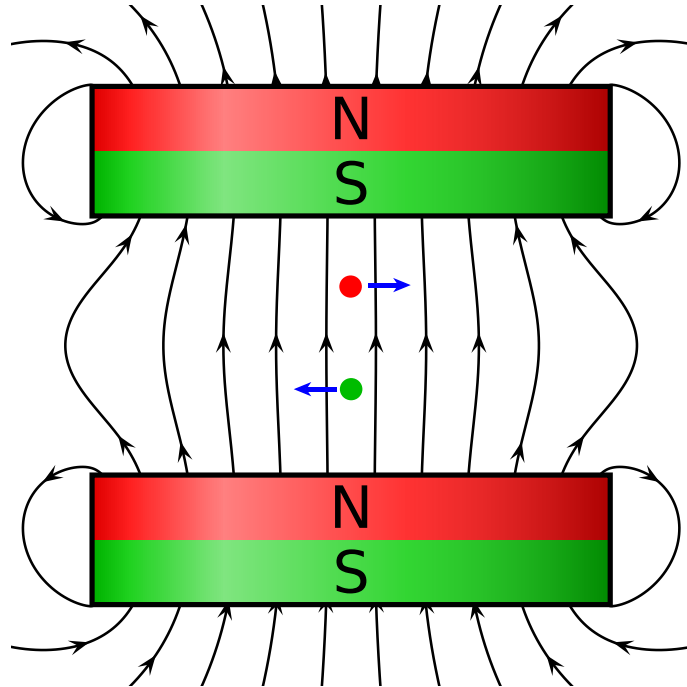


Figure 1.2: A representation of a pair of idealised cylindrical magnets in a dipole configuration. Two positively charged particles are shown as circles, the red particle is traveling out of the page, the green particle is traveling into the page. The forces experienced by each particle due to the magnetic field are shown as blue arrows.

The force which accelerates the particles is provided by radio-frequency cavities such as in figure 1.3, of which the LHC has 16 [1] The electric field in the radio-frequency cavity forms a standing wave, the separation between bunches of particles to be accelerated must be matched to the frequency of this wave. Protons in the LHC are accelerated in bunches and in vacuum, this to increase the likelihood of collisions and mitigate loss of energy and scattering effects due to interactions with air molecules. These two factors lead to the occurrence of space charge which causes an increase in the emittance of the beam, where the emittance is defined as the total area that the beam occupies in its beam-pipe. The greater the energy of the particles the more they can overcome increase in emittance due to space charge. Increased

emittance is especially problematic in circular accelerators where periodic effects can quickly lead to the loss of beam. For these reasons it would be very challenging to accelerate protons from rest in a synchrotron, the starting point for the protons of the LHC is therefore a linear accelerator called Linac2 [?] which is used to overcome space charge effects before the protons move on to a series of synchrotrons.

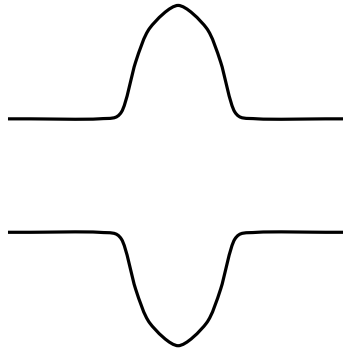


Figure 1.3: A representation of a radio-frequency cavity where the electric field lines are shown in black.

Even a beam with its emittance under control would still be lost from the accelerator if only dipole magnets were used to control its path. Magnets in a quadrupole configuration as in figure 1.4 are used to focus the beam and keep it in the beam-pipe. The quadrupoles behave such that particles feel a force that increases with the distance from the centre of the beam leading to simple harmonic motion of individual particles in a bunch. The LHC has a series of 24 quadrupole magnets each for focusing in the horizontal and vertical directions [1] as well as higher multipolarity configurations; sextupole, octupole, decapole and dodecapole which are used to correct imperfections in the fields of other magnets.

The statistical nature of particle physics analyses means that larger datasets (more recorded collisions) increase the sensitivity of searches and measurements. Constraints on the number of years the LHC is able to run mean that the best way to record more collisions is to collide more particles per second. A quantity known as the luminosity is often used to describe how much data is available for an analysis, it is written as

$$L = \frac{1}{\sigma} \frac{dN}{dt}, \quad (1.2)$$

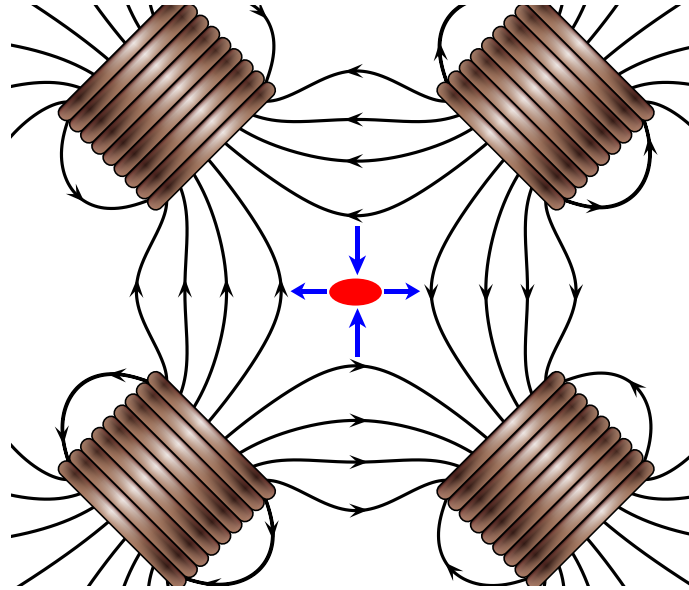


Figure 1.4: Representation of an idealised set of coil magnets in a quadrupole configuration with a proton beamspot shown as a red ellipse. The proton beam is drawn coming out of the page (*watch out!*), magnetic field lines are drawn in black and the forces acting on each bunch of protons are drawn as blue arrows.

where σ is the cross-section, a volume within which particles must pass by one another in order to interact, and N is the number of events recorded in a period of time t . For luminosity at the LHC N can be expressed as

$$N = n_{bp}n_1n_2\nu_r, \quad (1.3)$$

where n_{bp} is the number of colliding bunch pairs, n_1 and n_2 are the number of protons in each beam and ν_r is the frequency with which the beams rotate around the LHC's circumference. The number of particles in the beams is limited by space charge. The number of bunches is limited by the frequency that the radio-frequency cavities can operate at. The revolution frequency is limited by the strength of the dipole magnets and the circumference of the accelerator ring. Increasing luminosity by reducing the cross-section amounts to reducing the beam widths which is limited by the emittance of the beam. The LHC has already exceeded its design luminosity providing physicists with more data to analyse than expected and plans are well underway for the upgrade to a High-Luminosity LHC (HL-LHC) [11].

1.2 The ATLAS Detector

The ATLAS detector [12] resides at a location on the LHC ring called Point 1, its full name is A Toroidal LHC ApparatuS. A diagram of the detector is shown in figure 1.5. ATLAS is considered to be a general purpose particle detector and has a wide physics program including: Higgs boson physics, top quark physics, searches for Supersymmetry and exotic states, probes of CP violation in b-quarks and light states and heavy ion physics. The detector itself is very large in size, spanning a width of 25 m and a length of 44 m and weighs 7000 tonnes which is comparable to the weight of the wrought iron content of the Eiffel tower [13].

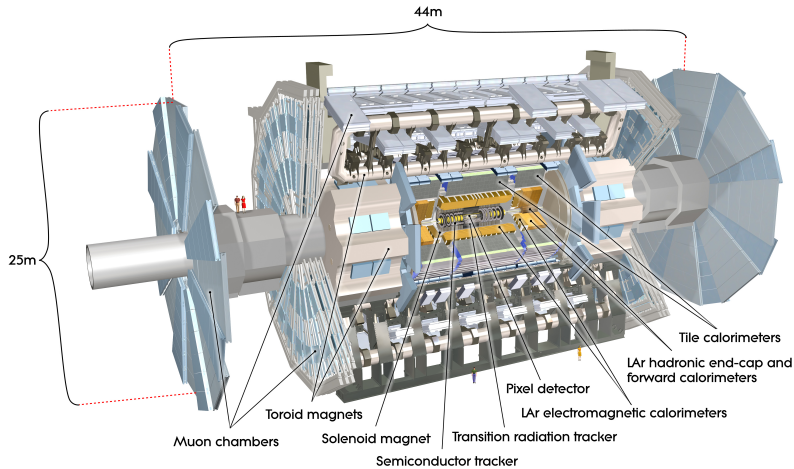


Figure 1.5: Computer generated image of the whole ATLAS detector with the major sub detectors labeled [14].

Due to the composite nature of the proton, the decay products of collisions are extremely numerous. Additionally when two bunches of protons cross there is the chance that more than one hard scattering event occurs and softer glancing collisions are also a possibility. The number of hard scattering events in a given bunch crossing is known as the pile-up of the collision and is often denoted with the symbol μ . As can be seen by inspecting equations 1.3 and 1.2 increasing the luminosity will often cause a higher pile-up environment in the detector. The variety of decay products available High pile-up, along with the numerous decay products of each collision necessitate the use of specialised sub-detectors in order to accurately measure the

output of collisions. For certain types of decay product there are different dedicated sub-systems in ATLAS with the purpose of measuring properties of particles of that type. At this stage it is sufficient to say that the treatment of electrically charged particles must be different to those that are electrically neutral, but this concept will be expanded upon in more detail in the further sections. It is interesting to note that despite the many charges that are associated with the forces of nature discussed in chapter ?? the only one that we can directly measure is electric charge.

The ATLAS sub-systems are located in either the barrel of the detector or one of the end-caps. These two areas have a different geometry and so the design of a sub-system in the barrel will differ from the same sub-system in the end-cap. What follows is a description of the ATLAS sub-systems and their individual components, for each component more detail will be given about which properties of which types of particles it is used to measure. These details are based on the ATLAS technical design report volumes [15, 16] unless another citation is present. Before detailing individual components it is important to detail certain properties of the detector relevant to all sub-systems. The coordinate system used to describe the ATLAS detector is known as right-handed. Three orthogonal axes (x, y, z) are used to describe the 3D space of the detector. The x-axis points towards the centre of the LHC ring, the y-axis points upwards and the z-axis points along the LHC beam pipe y-axis. The three axes meet at the interaction point which is the nominal position where bunches cross, located in the centre of the detector. Cylindrical coordinates (r, ϕ) are also often used to describe the physical features of the detector and phenomena caused by interactions in the detector that shall be referred to as analysis objects. Their definitions are that ϕ is the azimuthal angle in the x-y plane (transverse) around the beam pipe and r is the distance from the interaction point. A final quantity used due to its compatibility with description relativistic objects in the detector is pseudo-rapidity $\eta = -\ln(\tan(\theta/2))$ where θ is the zenith angle measured from the z-axis.

The grouping of particles into electrically charged or neutral is largely due to the

fact charged particles experience the Lorentz force

$$\vec{F} = q(\vec{E} + \vec{v} \times \vec{B}), \quad (1.4)$$

whereas neutral particles have $q = 0$, and so they do not. The magnetic field \vec{B} has the effect of changing the direction of the particles trajectory only. This is due to the fact that any force \vec{F} resulting from the cross product of two vectors, in this case the field vector and the velocity \vec{v} , must act in a perpendicular to the two crossed vectors and thus perpendicular to the direction of the motion (the direction of velocity). Similarly the electric field term \vec{E} has the effect that the particle is accelerated in the direction (or opposite in the case of a negative particle) of the field lines. The consequence of this is that in a known magnetic field the velocity of a particle can be calculated by measuring the radius of curvature of its trajectory. In order to exploit these properties of charged particles a large portion of the ATLAS detector is immersed in magnetic fields created by the magnet systems. There are four magnet systems in ATLAS the solenoid, the barrel toroid, and two end-cap toroids. The solenoid surrounds the inner detector whilst the toroid systems surround the muon chambers. Figure 1.6 shows a heat map of the magnetic field strengths within ATLAS, the image is from an article detailing the superconducting magnet system [17]. The magnet systems store a total energy of 1.6 GJ and produce fields of a combined volume of approximately $12 \times 10^4 \text{ m}^3$.

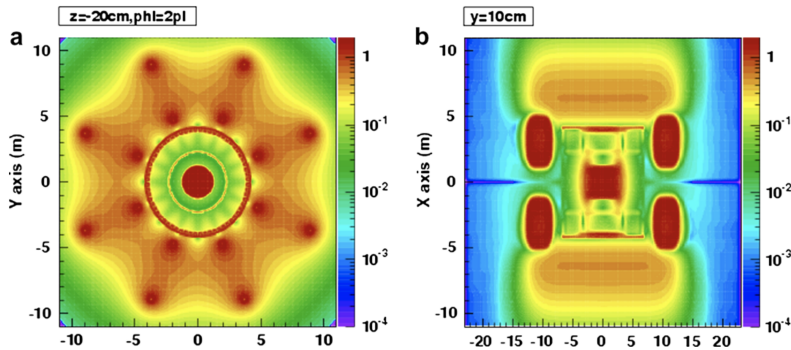


Figure 1.6: ATLAS magnetic field profile, showing a transverse cross-section in the centre of the detector (a), and a longitudinal section (b) [17].

Inner Detector

The Inner Detector (ID) is comprised of pixel detectors, the semiconductor tracker (SCT) and a transition radiation tracker (TRT) as seen in figure 1.7. It covers a volume corresponding with the total ϕ angle. In relation to η the pixel detectors and SCT cover the range $|\eta| < 2.5$ and the TRT covers $|\eta| < 2.0$. Being the innermost sub-detector of ATLAS the primary goals of the ID are to reconstruct the locations of the origin of interactions (known as the interaction vertex), and to track the propagation of charged particles through the detector. This is achieved by measuring a sequence of hits for each charged particle that propagates through its material, upon which reconstruction algorithms can be applied, known as track finding algorithms. From this sequence of hits interaction vertices can also be reconstructed, the vertex which comes from the highest energy collision in a given event is known as the primary vertex. Information from the tracker is used to match activity in outer regions of the detector to an interaction vertex. Each reconstructed track will have a momentum assigned to it, which is calculated using equation 1.4. The magnetic field that the ID is immersed in is produced by the solenoid magnet system. The system is made of a single layer coil with an inner diameter of 2.46 m and produces 2 T field in the axial direction with respect to the beam-pipe.

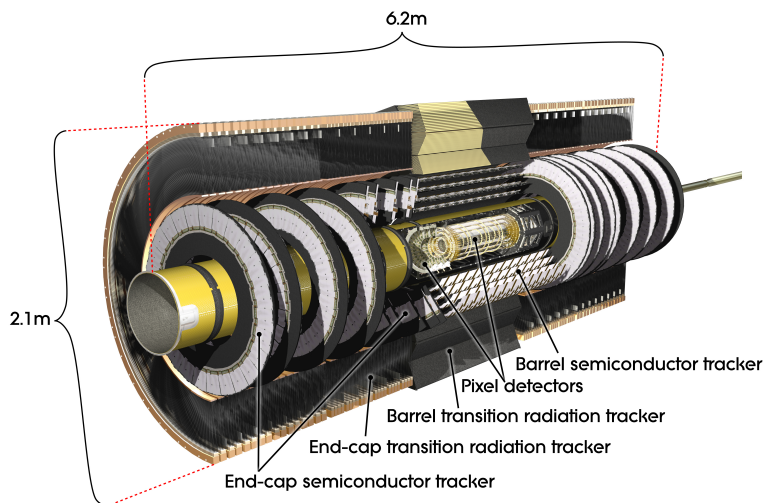


Figure 1.7: Computer generated image of the ATLAS inner detector [18].

Pixel Detectors

There are four layers of pixel detectors that are the closest components of the ID to the beam-pipe. The design originally had three layers, each $250\ \mu\text{m}$ thick with $50\ \mu\text{m}$ by $250\ \mu\text{m}$ pixels, of oxygen doped n-type silicon crystals. During LS1 a fourth layer, closest to the beam-pipe (which was also replaced for a smaller radius version) was added. This layer is known as the insertable B-layer (IBL) [19], the motivation for its addition was to counteract degradation of original performance of the ID due to irreversible damage by radiation. As well as the inclusion of the IBL, performance degradation is mitigated by increasing the bias voltage across the pixels from 100 V (their starting voltage) to up to 600 V. Additionally the IBL being closer to the beam-pipe allows for interaction vertices to be measured more precisely. The need for better reconstruction of vertices is motivated by their role in the performance of algorithms that classify jets of activity in the detector that are initiated by B-hadrons, this is where the IBL gets its name. There are no pixel detectors in the end-caps.

Semiconductor Tracker

Next closest to the beam-pipe are the semiconductor trackers. Similarly to the pixel detectors the semiconductor trackers are also made of silicon. In contrast to the n-type silicon of the pixels, the semiconductor trackers use p-in-n type technology. The semiconductor modules are comprised of two back to back silicon wafers that are offset by a small angle in order to improve coverage. Each wafer has a series of strips of p-in-type material covered in a metalised layer, the strips are separated by a distance of $80\ \mu\text{m}$. The strips have a bias voltage applied and on the wafers the necessary electronics are mounted for readout as seen in figure 1.8. In order to calibrate the response of the strips a $100\ \text{M}\Omega$ poly-silicon resistor is located at the end of each strip. Figure 1.9 shows an image of the snake-like structure of a poly-silicon resistor from the end of an SCT module. The modules come in two different designs, short strips and long strips with the short strips forming the layer

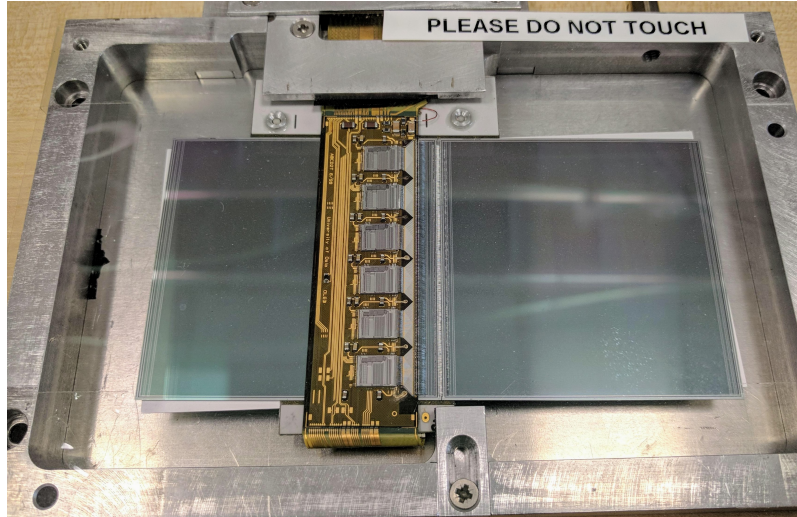


Figure 1.8: An image of an SCT long strip module mounted in a rig for testing at Queen Mary University of London.

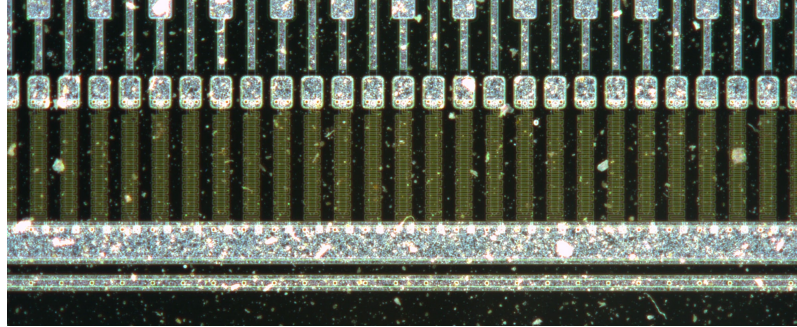


Figure 1.9: A close up image of the end of an SCT sensor in which the snake-like poly-silicon resistors are visible as a yellowish coloured structure at the end of each strip. This image was taken with a high resolution automatic area scanner commissioned by the author [20] in order to take full scans of strip sensors during the production of the ATLAS Inner Detector upgrade known as the Inner Tracker (ITk) [21, 22].

closest to the pixel detectors and the long strips on the outside.

The original operating bias voltage was 150 V but again due to radiation exposure this will raise to up to 350 V over time as necessary. There are four layers of semiconductor trackers in the barrel arranged so that sensors have a tilt with respect to a perfect coaxial cylinders of approximately 11 °. This tilt increases the amount of material that particles will travel through and is optimized to the geometry of the detector. Similarly the end-cap modules are arranged in petal like structures, with a number of different geometric designs based on the position within the end-cap.

Transition Radiation Tracker

The final layer of the ID is the TRT, the primary role of the TRT is to aid electron identification by measurement of transition radiation. The TRT is mostly made up of polyimide drift tubes with a diameter of 4 mm. The drift tubes are filled with a gas mixture whose majority constituent is xenon. These tubes operate with a voltage of -1530 V and are contained within a carbon fibre support structure. The geometrics layout of the tubes is optimized for both the barrel and end-caps.

Calorimeters

The purpose of the calorimeters is to measure the total energy of particles that pass all the way through the ID, this is achievable only if the calorimeter stops the particle completely. A desirable side effect is that they also act as a barrier to stop particles passing through to the muon spectrometers, of course this means necessarily that muons pass through the calorimeters. There are two calorimeter systems in ATLAS the electromagnetic calorimeter (ECAL) and the hadronic calorimeter (HCAL), they will be explained in the following sections. The calorimeters are not immersed in a significant magnetic field compared to the rest of the ATLAS as seen in the heat map of figure 1.6. This is because measuring the energy of

particles and acting as a barrier to them does not require curved trajectories. The geometric layout of the calorimeter systems, as well as the location of specific components can be seen in figure 1.10, in which the ID can also be seen (greyed out). Information from the two calorimeters is used in conjunction for any particles whose decay products propagate through both volumes. Both calorimeters are split up into cells of material that are used to determine the position of decay products in the detector.

Electromagnetic Calorimeter

The ECAL is primarily concerned with measuring the energy and stopping the trajectory of electrons and photons. It has liquid argon (LAr) as it's active material.

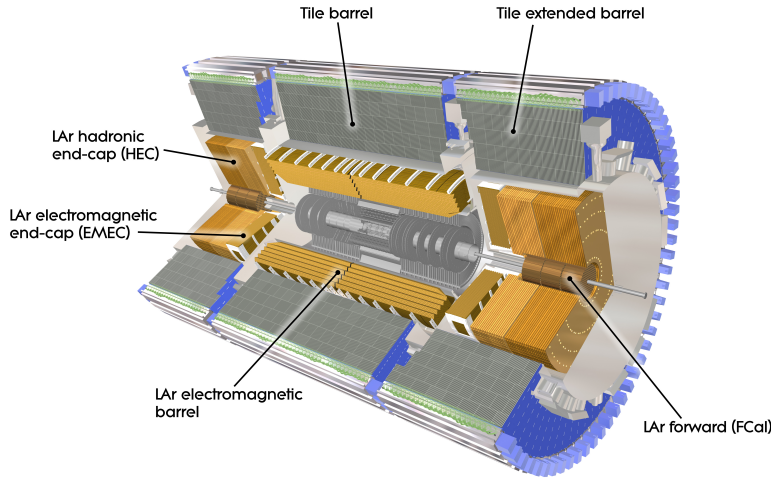


Figure 1.10: Computer Generated image of the ATLAS calorimeter [23].

Particles initiate an electromagnetic shower of decay products in the active material which ionizes it. An applied electric field causes these ions to drift in such a way that the current induced is proportional to the energy deposited by the incident particle.

Hadronic Calorimeter

The HCAL also has a LAr component which works in a similar way to that of the ECAL but with different optimizations for the HCAL's specialised design. The HCAL is specifically tasked with measuring the energy and stopping the trajectory of hadrons. The HCAL also contains a tile calorimeter which uses scintillation light produced in the tiles as a means to measure the deposited energy of hadrons.

Muon Spectrometers

Surrounding the calorimeters are the muon spectrometers, which form the most outer layer of the detector. Though muons are charged leptons just like electrons, their specific properties mean that dedicated muon spectrometers are required to detect them. Muons deposit far less energy per distance traveled than other particles meaning that they punch through most materials with ease. As can be seen in figure 1.11 the components of the muon spectrometers are the thin-gap chambers,

cathode strip chambers, resistive plate chambers and monitor drift tubes. The barrel and end-cap toroid magnets immerse the muon spectrometers in a magnetic field which at its peak (visible in figure 1.6) has a strength of 4 T. Despite a stronger peaking magnetic field than in the solenoid observed muon tracks are often far less curved than that of their lighter cousins, the electrons. This is due to the larger mass of the muon. Muons do leave tracks in the ID and also deposit small amounts of energy in the calorimeters. Tracks in the muon spectrometers are matched up to tracks in the ID with the aid of the location of energy deposits in the calorimeters if possible. The full tracking information for muons can be used in algorithms such as overlap removal, which is used to remove muons from jets that they have been erroneously associated with by matching the muon with its ID track.

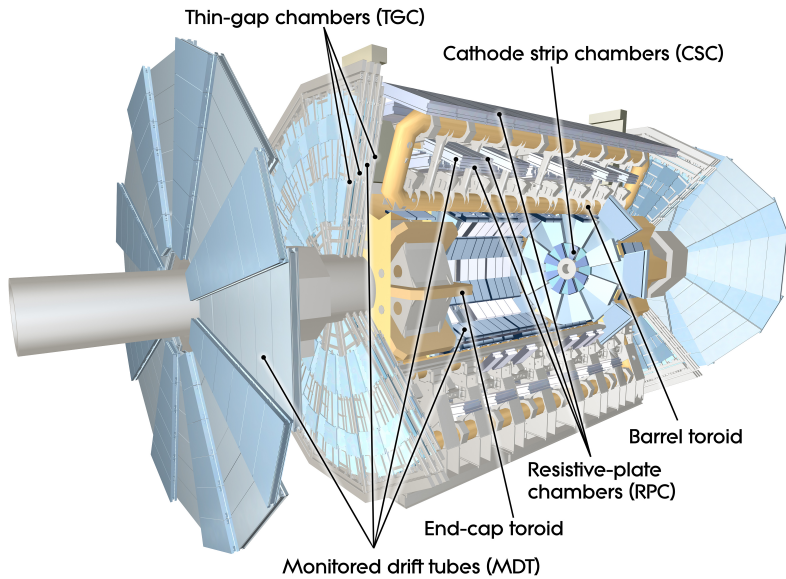


Figure 1.11: Computer generated image of the ATLAS Muons subsystem [24].

Trigger Systems

The trigger systems in ATLAS allows data to be recorded only when an event meets certain criteria. Without triggering there would be no way to decide which events to readout and which to ignore. It would be impossible to readout every interaction that occurs in the detector. The reason for this is that the geometric constraints of the detector mean that there is only a small space available for readout wires, as

detection medium needs to be prioritized for sensitivity and technology limits the data rate that one can achieve through a cable of fixed area. The trigger system comes in two parts, a hardware component referred to as level one (L1) and software component referred to as the high level trigger (HLT). The L1 system is comprised of the L1 calorimeter (L1Calo) trigger which operates by searching for clusters of energy in the calorimeters and the L1 muon (L1Muon) system which coincidences in the muon systems. A third system L1 topological (L1Topo) uses regions of interest built from the L1Calo and L1Muon data which are passed to central trigger processors for selection. The various limitations of the hardware mean that these selections must be passed up to the next level of triggering, the HLT in a time window of $2.5 \mu\text{s}$. The HLT takes information from the L1 systems and uses faster versions of an offline style analysis in order to select or reject events for readout. In order for a trigger to fire an event must pass fully all of the requirements of one of the algorithms defined by an extensive trigger menu. More information about the triggers used in the $VH(bb)$ analysis will be given in a later chapter.

Bibliography

- [1] Oliver Sim Brüning, Paul Collier, P Lebrun, Stephen Myers, Ranko Ostojic, John Poole, and Paul Proudlock. *LHC Design Report*. CERN Yellow Reports: Monographs. CERN, Geneva, 2004. URL <https://cds.cern.ch/record/782076>.
- [2] *LEP design report*. CERN, Geneva, 1984. URL <https://cds.cern.ch/record/102083>. Copies shelved as reports in LEP, PS and SPS libraries.
- [3] CERN. ATLAS: Letter of intent for a general purpose p p experiment at the large hadron collider at CERN. 1992.
- [4] M. Della Negra et al. CMS: letter of intent by the CMS Collaboration for a general purpose detector at LHC. Technical Report CERN-LHCC-92-003. LHCC-I-1, CERN, Geneva, 1992. URL <https://cds.cern.ch/record/290808>. Open presentation to the LHCC 5 November 1992, M. Della Negra/CERN, CMS Spokesman.
- [5] H. Dijkstra, Hans Jürgen Hilke, Tatsuya Nakada, and Thomas Ypsilantis. LHCb Letter of Intent, LHCb Collaboration. 1995.
- [6] Letter of Intent for A Large Ion Collider Experiment [ALICE]. Technical Report CERN-LHCC-93-016. LHCC-I-4, CERN, Geneva, 1993. URL <https://cds.cern.ch/record/290825>.
- [7] G Giacomelli, A A Faust, and James L Pinfold. A search for highly ionizing particles and slow exotic decays at the LHC using the MOEDAL detectors:

- letter of intent. Technical Report CERN-LHCC-98-05. LHCC-I-19, CERN, Geneva, Feb 1998. URL <https://cds.cern.ch/record/347906>.
- [8] W Kienzle, , et al. *Total cross section: elastic scattering and diffraction dissociation at the LHC.* Letter of Intent. CERN, Geneva, 1997. URL <http://cds.cern.ch/record/335255>.
- [9] O Adriani. LHCf Letter of Intent for a p-Pb run. A precise study of forward physics in $\sqrt{s_{NN}} = 4.4$ TeV proton-Lead ion collisions with LHCf at the LHC. Technical Report CERN-LHCC-2011-015. LHCC-I-021, CERN, Geneva, Dec 2011. URL <https://cds.cern.ch/record/1404163>.
- [10] Christiane Lefèvre. The CERN accelerator complex. Complexe des accélérateurs du CERN. Dec 2008. URL <https://cds.cern.ch/record/1260465>.
- [11] I. Bejar Alonso and L. Rossi. HiLumi LHC Technical Design Report. 2015.
- [12] Georges Aad et al. (ATLAS Collaboration). The atlas experiment at the cern large hadron collider. *Journal of Instrumentation*, 3(08):S08003, 2008. URL <http://stacks.iop.org/1748-0221/3/i=08/a=S08003>.
- [13] David Hanser. *Architecture of France*. Greenwood Press, Westport, Conn, 2006. ISBN 978-0-313-31902-0.
- [14] Joao Pequenao. Computer generated image of the whole ATLAS detector. Mar 2008. URL <https://cds.cern.ch/record/1095924>.
- [15] A. Airapetian et al. ATLAS: Detector and physics performance technical design report. Volume 1. 1999.
- [16] A. Airapetian et al. ATLAS: Detector and physics performance technical design report. Volume 2. 1999.
- [17] H.H.J. ten Kate. The atlas superconducting magnet system at the large hadron collider. *Physica C: Superconductivity*, 468(15):2137 – 2142, 2008. ISSN 0921-4534. doi: <https://doi.org/10.1016/j.physc.2008.05.146>. URL <http://>

- www.sciencedirect.com/science/article/pii/S0921453408004541. Proceedings of the 20th International Symposium on Superconductivity (ISS 2007).
- [18] Joao Pequenao. Computer generated image of the ATLAS inner detector. Mar 2008. URL <https://cds.cern.ch/record/1095926>.
- [19] M Capeans, G Darbo, K Einsweiller, M Elsing, T Flick, M Garcia-Sciveres, C Gemme, H Pernegger, O Rohne, and R Vuillermet. ATLAS Insertable B-Layer Technical Design Report. Technical Report CERN-LHCC-2010-013. ATLAS-TDR-19, Sep 2010. URL <https://cds.cern.ch/record/1291633>.
- [20] Thomas Paul Charman, Bart Hommels, and Adrian John Bevan. Authorship Qualification Task: ATLAS ITk Sensor Scanner Documentation (QMUL). Technical Report ATL-COM-ITK-2019-018, CERN, Geneva, Jan 2019. URL <https://cds.cern.ch/record/2674404>.
- [21] Ben Brueers. The design and layout of the Phase-II upgrade of the Inner tracker of the ATLAS experiment. Jul 2019. URL <https://cds.cern.ch/record/2681301>.
- [22] John Stakely Keller. The ATLAS ITk Strip Detector System for the Phase-II LHC Upgrade. Feb 2019. URL <https://cds.cern.ch/record/2663172>.
- [23] Joao Pequenao. Computer Generated image of the ATLAS calorimeter. Mar 2008. URL <https://cds.cern.ch/record/1095927>.
- [24] Joao Pequenao. Computer generated image of the ATLAS Muons subsystem. Mar 2008. URL <https://cds.cern.ch/record/1095929>.